doi:10.4149/neo_2021_210806N1115

High level of TXNDC9 predicts poor prognosis and contributes to the NF-κB-regulated metastatic potential in gastric cancer

Qun-Cao YANG, Nan HAO, Rui-Hua LI, Yuan-Yuan DUAN, Yong ZHANG*

Department of Surgical Oncology, The First Affiliated Hospital of Xi'an Jiaotong University, Xi'an, Shanxi, China

**Correspondence: zhangyongzydr@yeah.net*

Received August 6, 2021 / Accepted October 26, 2021

Gastric cancer (GC) is the most frequent malignant tumor in the digestive system, with high metastasis potential and poor prognosis. This study aimed to investigate the prognostic value and biological function of thioredoxin domain-containing protein 9 (TXNDC9) in GC. The expression of TXNDC9 was analyzed based on The Cancer Genome Atlas (TCGA) database. The prognostic value of TXNDC9 was evaluated by Kaplan-Meier curves and Cox regression analysis. The mRNA and protein expression of TXNDC9 were analyzed using quantitative real-time PCR and western blot analysis. The effects of TXNDC9 on GC cell invasion and EMT were assessed *in vitro*, and its effects on tumorigenesis were confirmed using animal experiments. The activity of the NF-κB signaling pathway was examined by both *in vitro* and *in vivo* experiments. TXNDC9 was highly expressed in GC tissues and cell lines. A high level of TXNDC9 was associated with poor overall survival and served as an independent prognostic biomarker in GC patients. The knockdown of TXNDC9 led to restrained GC cell invasion, microtubule formation, and EMT *in vitro*, and suppressed tumorigenesis *in vivo*. In addition, the NF-κB signaling pathway was demonstrated to mediate the functional role of TXNDC9 in GC. In conclusion, this study found that high TXNDC9 predicted poor prognosis in GC, and served as an oncogene by enhancing tumor cell invasion and EMT through the NF-κB signaling pathway.

Key words: gastric cancer, differentially expressed genes, thioredoxin domain-containing protein 9, prognosis, metastasis, epithelial-mesenchymal transition, NF-κB signaling pathway

Gastric cancer (GC) is a commonly occurring aggressive human malignancy, ranking the fourth most frequent malignant tumor and the second leading cause of mortality due to cancer worldwide [1]. Despite advances in therapeutic strategies, GC is still difficult to cure, mainly owing to that most GC patients are initially diagnosed with advanced tumors or positive metastasis [2]. Currently, based on tumor progression and individual differences, GC patients receive personalized treatment, including surgery, chemotherapy, and radiotherapy [3]. However, the survival outcomes of GC patients remain not ideal. Thus, more efficient therapeutic strategies are urgently necessary for the treatment of GC. Molecular targeted therapy has been highlighted in cancer treatment in recent years, which is achieved by exploring key genes in the progression of various tumor progression [4]. Therefore, finding more functional molecules in carcinogenesis may provide novel insight into targeted therapies in GC.

The thioredoxin (TRX) family contains a series of redox proteins, which can catalyze the reversible oxidation of cysteine mercaptan to disulfide [5]. The proteins in this family have some important biological functions, such as the regulation of oxidative stress, redox homeostasis, and transcription [6, 7]. Of note, the TRX family has been found to play promoting effects on tumorigenesis in some malignancies [5, 8]. Thioredoxin domain-containing protein 9 (TXNDC9), as a member of the TRX family, is also named phosducin-like protein 3 (PHLP3), which has a critical regulatory function in ATPase activity [9]. Recently, the role of TXNDC9 in cancers has been investigated, and the upregulated TXNDC9 has been documented to play as an oncogene in the tumor progression in prostate cancer [10], hepatocellular carcinoma [11], glioma [12], and colorectal carcinoma [10]. In addition to the functional role of TXNDC9, it has been reported that the increased TXNDC9 expression could predict a poor prognosis of colorectal carcinoma [13]. However, the understanding of the relationship of TXNDC9 with GC prognosis and progression remains limited.

In this study, the expression and prognostic value of TXNDC9 were evaluated based on the data from The Cancer Genome Atlas (TCGA) database. Next, this study investi-

gated the regulatory effects of TXNDC9 on GC cell invasion, tubule formation, and epithelial-mesenchymal transition (EMT), and further analyzed the underlying mechanisms. The analysis results may provide evidence for TXNDC9 as a novel prognostic indicator and a potential therapeutic target in GC.

Materials and methods

Bioinformatics analysis. This study used the ACLBI (https://www.aclbi.com/static/index.html#/) to analyze the data from TCGA database (https://portal.gdc.cancer.gov/). The expression of TXNDC9 in 375 GC tissues and 391 normal controls was compared, and the Kaplan-Meier survival curves for GC patients were plotted based on different TXNDC9 expressions.

Cell culture. Five GC cell lines, including SGC-7901, BGC-823, AGS, MGC-8032, and MKN-1, a human normal gastric epithelial cell line GES-1 and human umbilical vein endothelial cells (HUVECs) were purchased from the Type Culture Collection of the Chinese Academy of Sciences (Shanghai, China) and cultured in Dulbecco's modified Eagle's medium (DMEM; HyClone, Logan, UT, USA) supplemented with 10% fetal bovine serum (FBS; Gibco, Logan, UT, USA), 100 U/ml penicillin and 100 μg/ml streptomycin (Invitrogen, Carlsbad, CA, USA) at 37 °C in a humidified atmosphere with 5% CO_2.

Cell transfection and treatment. The short hairpin RNAs (shRNAs) against TXNDC9, including TXNDC9-shRNA1, TXNDC9-shRNA2, and TXNDC9-shRNA3, and the corresponding negative control (shRNA-NC) were synthesized from GenePharma (Shanghai, China). To knock down TXNDC9, the synthesized shRNAs were transfected into AGS and MKN1 cells using Lipofectamine 3000 Transfection Reagent (Invitrogen, Carlsbad, CA, USA) according to the manufacturer's instructions. AGS cells were stimulated with LPS at a concentration of 10 μg/mL for 24 h to enhance cell migration and invasion abilities [14]. After 24 h of cell transfection with sh-TXNDC9, the cells were subjected to LPS stimulation.

RNA extraction and quantitative real-time PCR (qRT-PCR). Total RNA was extracted from the analyzed cells using Trizol (Invitrogen, Carlsbad, CA, USA). The purity of RNA was confirmed by calculating the ratio of OD260/OD280, and the ratio closed to 2.0 indicated that the RNA could be used for further analysis. Single-stranded cDNA was synthesized from 1 μg RNA using a Promega cDNA core kit (Promega, Madison, WI, USA) following the protocols of the manufacturer.

The relative mRNA expression of TXNDC9 was evaluated using qRT-PCR, which was carried out using SYBR Premix ExTaq (TaKaRa Bio, Kusatsu, Japan) on a 7500 real-time PCR system (Applied Biosystems, Foster City, CA, USA). The reactions were performed using the following program: 95 °C for 10 min, 40 cycles of 95 °C for 30 s, 60 °C for 20 s, 72 °C for 30 s. GAPDH was used as an internal control, and the relative expression results were computed using the $2^{-\Delta\Delta Ct}$ method. Following were the sequences of primers: TXNDC9 forward: 5'-CTGCTTCAGACTACCAAACTGG-3', reverse: 5'-CTCTGTAGAAATGGCAAACCACA-3'; GAPDH forward: 5'-ATCAGCAATGCCTCCTGCAC-3', reverse: 5'-CGTCAAAGGTGGAGGAGTGG-3'. Each sample was detected 3 times.

Western blot analysis. The protein expression in AGS and MKN1 cells and tumor tissues was measured using western blot analysis. Total proteins were collected by RIPA lysis buffer (Beyotime, Shanghai, China), then were quantified using a BCA Protein Quantitation Kit (Thermo Fisher, Waltham, MA, USA). Sodium dodecyl sulfate-polyacrylamide gel electrophoresis (SDS-PAGE) (10%) was used to separate proteins, then the proteins were transferred to polyvinylidene fluoride (PVDF) membranes (Millipore, Billerica, MA, USA). The primary antibodies (Santa Cruz Biotechnology, CA, USA), including anti-TXNDC9 (1:100, #sc-514770), anti-VEGF (1:200, #sc-7269), anti-E-cadherin (1:200, #sc-8426), anti-N-cadherin (1:200, #sc-8424), anti-Vimentin (1:200, #sc-6260), anti-P65 (1:200, #sc-8008), anti-p-P65 (1:200, #sc-136548), anti-Bcl-2 (1:200, #sc- 7382), anti-TNF-α (1:200, #sc-12744), anti-MIP-1β (1:100, #sc-393441), and anti-GAPDH (1:200, #sc-47724), were incubated with the membranes at 4 °C overnight after membrane blocking with 5% skim milk. Next, the membranes were incubated with HRP-labelled secondary antibody (Jackson, PA, USA) at 37 °C for 2 h. In this analysis, GAPDH was used as a loading control. After that, an ECL system (Millipore, Billerica, MA, USA) was applied for protein band visualization, and the ImageJ software (NIH, Bethesda, MA, USA) was used to quantify the protein bands.

Transwell assay. The invasive ability of AGS and MKN1 cells was investigated using Transwell (BD Bioscience, NJ, USA). The upper chambers were pre-coated with Matrigel (BD Bioscience), and the lower chambers contained DMEM supplemented with 10% FBS. Cells with a density of 2×10^5 cells/well in serum-free culture medium were seeded into upper chambers and cultured for 24 h at 37 °C. After that, the cells in the upper chambers were removed, and the cells in the lower chambers were stained and counted under a light microscope with a magnification of ×100.

Microtubule formation assay. HUVECs with a density of 5×10^3 cells/well were seeded into a 24-well plate, which was precoated with Matrigel (BD Bioscience) and contained GC cell culture medium under indicated conditions. After incubation at 37 °C for 2 h, the number of nodes was counted in 5 random visual fields.

***In vivo* tumor formation.** Nude mice xenograft tumor models were performed in 10 SCID mice (aged 6–8 weeks, 5 mice in each group) by subcutaneously injecting TXNDC9-downregulated AGS cells (2×10^6 cells). The tumor volume was recorded every 5 days after inoculation. The volume of the tumor was calculated according to the formula $(a\times b^2)/2$, in which a meant the larger tumor dimension, and b meant the

smaller dimension. After 30 day-observation, the mice were sacrificed, and tumors were removed for further analyses. The tumor weight was evaluated, and the expression of TXNDC9, EMT conditions and the activity of nuclear factor kappa B (NF-κB) pathway were measured using western blot assay and immunohistochemistry (IHC) staining. The animal experiments were performed with the approval of the Animal Care and Use Committee of The First Affiliated Hospital of Xi'an Jiaotong University (SYXK(shan)2018-001).

IHC staining. The detailed procedures of IHC were in accordance with the methods previously described [15]. Briefly, tumor paraffin-embedded sections were deparaffinized and incubated in retrieval buffer to restore antigens. The protein expression of TXNDC9 and EMT markers was visualized using a Dako Real Envision Kit (Dako) after staining with primary antibodies (Santa Cruz Biotechnology, CA, USA), including anti-TXNDC9 (#sc-514770), anti-VEGF (#sc-7269), and anti-E-cadherin (#sc-8426). The IHC results were determined by the percentage of positively stained cells was determined by calculating the tumor cells in 5 random visual fields.

Statistical analysis. The data were expressed as mean ± SD and analyzed using the SPSS 21.0 software (SPSS Inc., Chicago, IL, USA) and GraphPad 7.0 software (GraphPad Software, Inc., USA). The comparisons between two groups were performed using Wilcoxon test and Student's t-test. The differences between multiple groups were assessed using Kruskal-Wallis test and one-way ANOVA followed by Bonferroni post hoc test. The survival curves of GC patients were plotted using Kaplan-Meier methods, and the different distribution between the curves was compared by log-rank test. The predictive accuracy of TXNDC9 was compared by time dependent receiver operating characteristic curve (ROC) analysis. The prognostic value of TXNDC9 was confirmed using univariate and multivariate Cox regression analysis, and a nomogram model was constructed based on the results from Cox analysis. The above survival analyses were performed using R software version v4.0.3. A p-value of less than 0.05 indicated statistically significant.

Results

Increased expression of TXNDC9 in GC patients. From TCGA database, TXNDC9 expression was analyzed in 375 patients with GC, and the clinical characteristics are listed in Supplement 1 and 2. As compared to the normal controls, tumor tissues had significantly high levels of TXNDC9 ($p<0.001$, Figure 1A). In addition, the expression of TXNDC9 in GC patients with different pN stages was compared, and it was found that the expression level of TXNDC9 was strongly upregulated in GC patients from stage N0 to N3 compared with normal controls, and the highest TXNDC9 levels were observed in cases with N2 stage ($p<0.001$, Figure 1B). These data indicated that TXNDC9 might play a role in GC development and progression.

Association of TXNDC9 with the overall survival of GC analyzed from TCGA database. Considering the differential expressions of TXNDC9 in GC patients, the relationship between TXNDC9 and GC survival was evaluated using the survival information of TCGA database. As shown in Figure 1C, the median survival time of GC patients with high TXNDC9 was shorter than those with low TXNDC9 (1.7 years vs. 4.5 years), indicating that high TXNDC9 was associated with poor overall survival (log-rank $p=0.00134$, HR=1.728, 95% CI=1.237–2.413). Moreover, the timeROCs showed that the area under the curve (AUC) was 0.575, 0.629, and 0.620 for TXNDC9 to predict the 1, 3, and 5-year survival of GC (Figure 1D). Furthermore, Cox regression analysis was conducted using the data listed in Supp. 2. The univariate Cox analysis results demonstrated that TXNDC9, age, pT, and pN stages were related with GC survival (all $p<0.05$, Figure 2A), and the multivariate Cox analysis indicated that TXNDC9, age, and pN stage were independent prognostic factors for GC patients (all $p<0.05$, Figure 2B). Finally, a nomogram model was constructed according to the variables screened from the multivariate Cox analysis (Figure 2C), and the C-index of the model was 0.673 (95% CI of 0.603–1, $p<0.001$). All the above results suggest that the aberrantly expressed TXNDC9 serves as an independent prognostic biomarker of GC.

Knockdown of TXNDC9 inhibits GC cell invasion and EMT. In addition to the clinical value of TXNDC9 in GC progression, this study focused on the biological function of TXNDC9 in GC progression. As shown in Figure 3A, the mRNA level of TXNDC9 was markedly augmented in 5 GC cell lines (SGC-7901, BGC-823, AGS, MGC-8032, and MKN-1) compared with the normal cell line GES-1 (all $p<0.05$), and the significant increase in TXNDC9 was observed in AGS and MKN1 cells ($p<0.001$ for AGS, $p<0.01$ for MKN1). Thus, AGS and MKN1 cells were used for the following cell experiments. By cell transfection, shRNAs against TXNDC9 significantly decreased the mRNA and protein expression of TXNDC9 in AGS and MKN1 cells (all $p<0.05$), and TXNDC9-shRNA1 exhibited the best inhibition results ($p<0.01$ for mRNA expression, $p<0.001$ for protein expression; Figures 3B–3D), which was used for subsequent experiments. For GC cell invasion, we found that the knockdown of TXNDC9 in both AGS and MKN1 cells led to the inhibited invasion and microtubule formation abilities (all $p<0.01$, Figures 3E, 3F). In addition, the reduction of TXNDC9 also attenuated the EMT of AGS and MKN1 cells, which was indicated by the decreased VEGF, N-cadherin, and vimentin, and increased E-cadherin protein levels (all $p<0.01$, Figure 3G).

TXNDC9 silencing inhibits GC cell invasion and EMT through the NF-κB signaling pathway. The current understanding of the mechanisms of TXNDC9 remains limited. The NF-κB signaling pathway plays a pivotal role in the carcinogenesis of GC [16]. In addition to the regulation of tumor cell proliferation, the NF-κB signaling pathway is associated with tumor cell motor abilities, inflammation, and

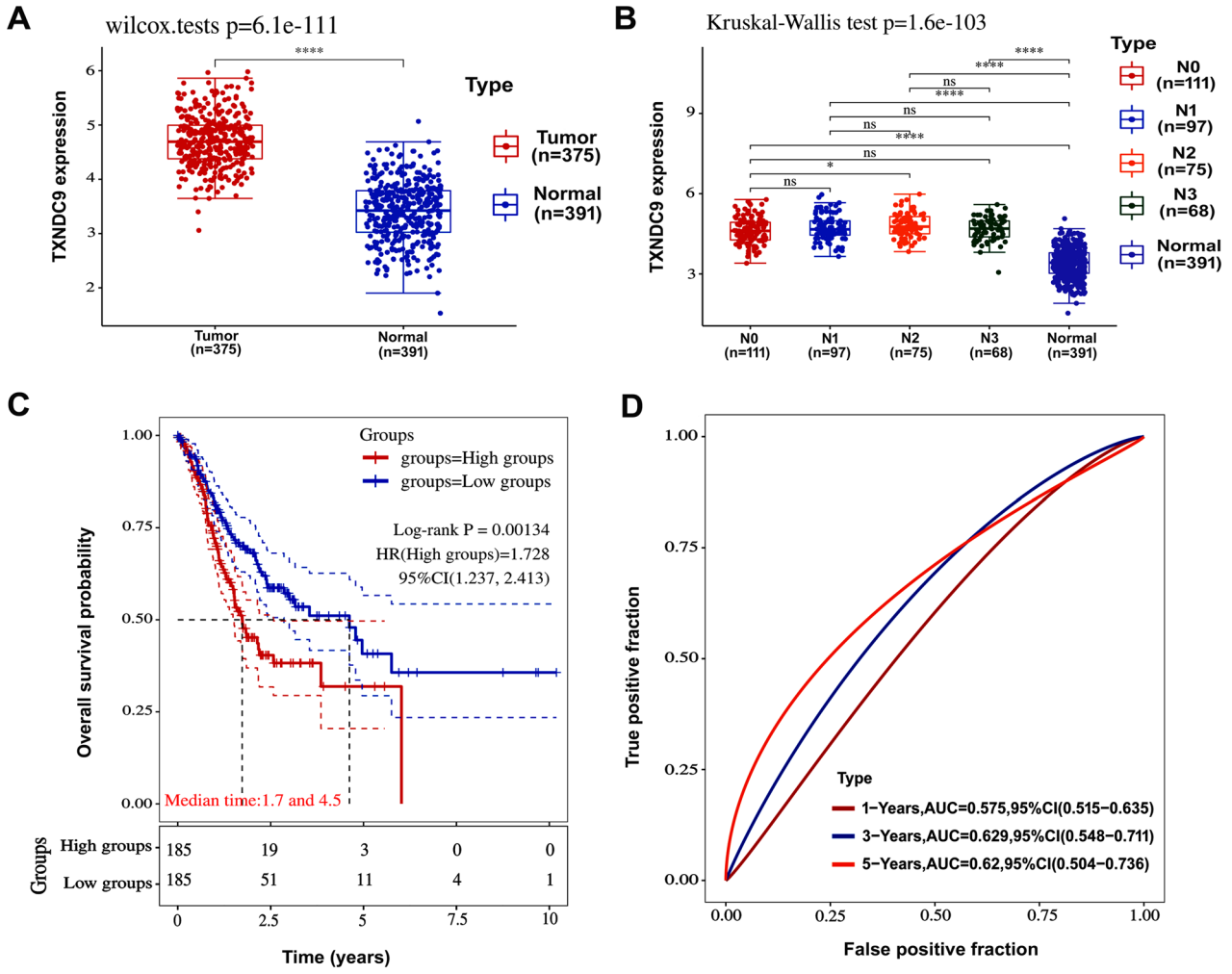

Figure 1. Expression of TXNDC9 and its relationship with overall survival in patients with GC. A) GC tissues (n=375) had significantly higher TXNDC9 expression than normal controls (n=391) (Wilcoxon test p=6.1e−111). B) GC patients were grouped into N0 (n=111), N1 (n=97), N2 (n=75), N3 (n=68) groups, and each group had significantly increased TXNDC9 levels compared with the normal controls (n=391) (Kruskal-Wallis test p=1.6e−103). C) Kaplan-Meier curves based on TXNDC9 expression for GC patients (log-rank p=0.00134). D) TimeROCs for TXNCD9 to predict 1, 3, and 5-year survival in GC patients (AUC, area under the curve).

the immune microenvironment in carcinogenesis. Thus, the effects of TXNDC9 on the activity of the NF-κB signaling pathway were investigated by analyzing related proteins. As shown in Figure 4A, TXNDC9 reduction could inhibit the ratio of p-P65/P65, the downstream protein levels of Bcl-2, TNF-α, and MIP-1β in both AGS and MKN1 cells (all p<0.01). LPS plays stimulative effects on tumor progression, especially on tumor cell migration and invasion, and the NF-κB pathway has been demonstrated to be a key mechanism of the processes [17]. By LPS treatment, the protein expression of TXNDC9 was significantly enhanced (p<0.01), while this effect was reversed by TXNDC9-shRNA1 (p<0.01, Figure 4B). As expected, the activity of NF-κB signaling was promoted by LPS (p<0.01), and the TXNDC9 knockdown abolished the promoting effects of LPS on the NF-κB signaling pathway (p<0.01, Figure 4C). In addition, the EMT, cell invasion, and microtubule formation abilities of AGS cells were all enhanced by LPS (all p<0.01), but TXNDC9 inhibition reversed these effects caused by LPS treatment (all p<0.01, Figures 4D–4H).

TXNDC9 knockdown suppresses tumorigenesis *in vivo*. The xenograft tumor model was constructed and the tumor weight and volume were inhibited under the condition of TXNDC9 inhibition (p<0.01, Figures 5A–5C). Besides, the protein expression level of TXNDC9 in the tumors was significantly decreased by TXNDC9-shRNA1, and TXNDC9 knockdown inhibited the levels of VEGF with enhanced E-cadherin expression (both p<0.01, Figures 5D, 5E). Furthermore, for the activity of the NF-κB signaling pathway, the silencing of TXNDC9 led to the inhibited ratio of p-P65/P65 and decreased levels of Bcl-2, TNF-α, and MIP-1β (all p<0.01, Figure 5F).

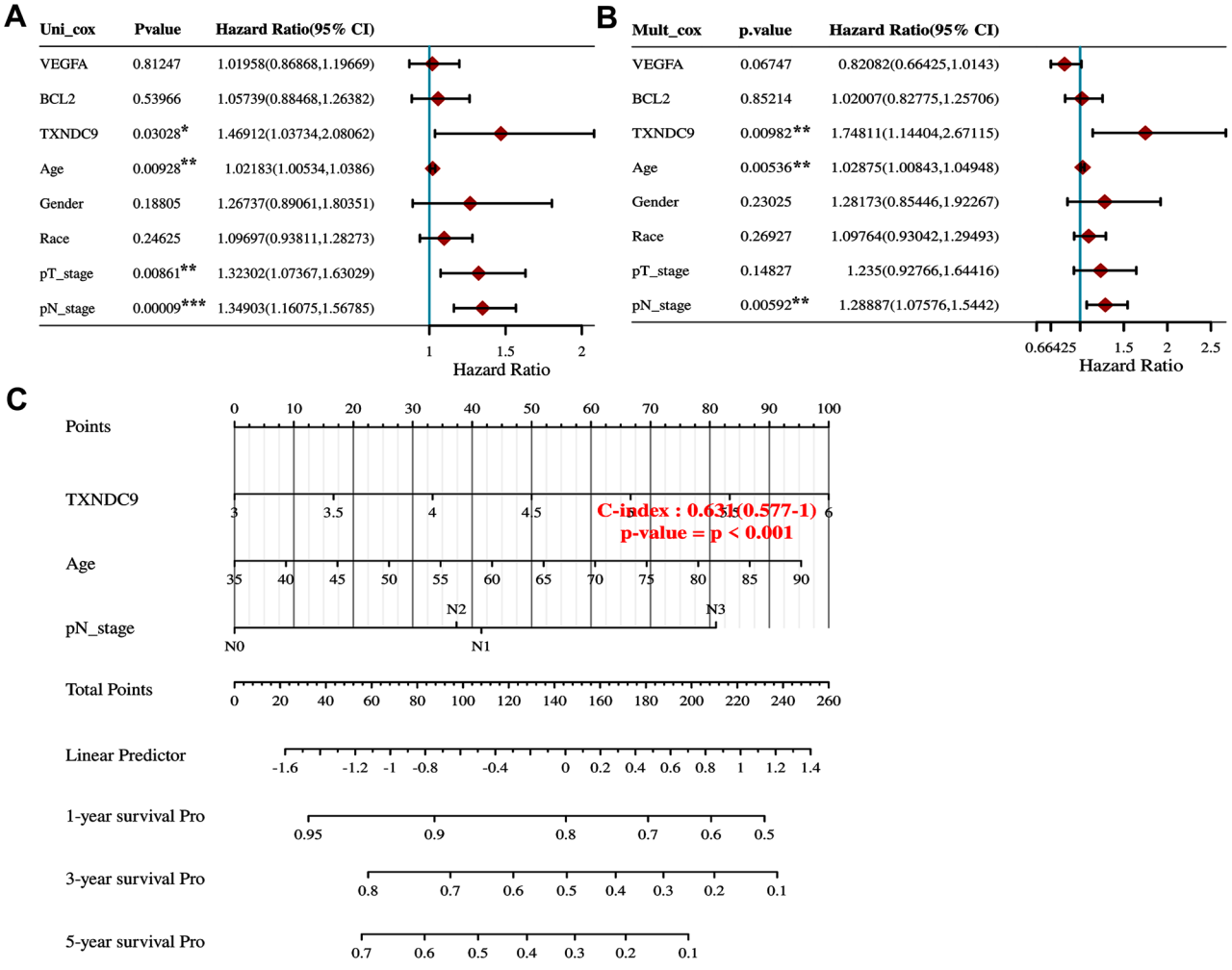

Figure 2. A nomogram survival model was constructed based on Cox regression analysis. A, B) Univariate and multivariate Cox regression analysis for TXNDC9, markers related to cell growth and metastasis, and other clinical variables. C. The nomogram was constructed based on TXNDC9, age, and pN stage (C-index = 0.673).

Discussion

Various differentially expressed molecules have been identified as key regulators in tumorigenesis in various human cancers, including GC [18]. This study analyzed expression data from TCGA database and found remarkably upregulated TXNDC9 in GC tissues compared with normal controls. In addition, high TXNDC9 was demonstrated to predict a poor prognosis of GC. In GC cell lines, the knockdown of TXNDC9 inhibited GC cell invasion, microtubule formation, and EMT, and the NF-κB signaling pathway was significantly inactivated by TXNDC9 reduction in GC cells. By *in vivo* animal analysis, TXNDC9 silencing was confirmed to inhibit the tumorigenesis of GC through the NF-κB signaling pathway.

A large number of studies have reported that differentially expressed molecules in tumor development and progression play pivotal roles in carcinogenesis [19]. In GC, some differentially expressed genes (DEGs) serve as oncogenes or tumor suppressors by promoting or inhibiting tumor progression. For example, the expression of prospero homeobox protein-1 (PROX1) was augmented in GC tissues, and GC patients with high PROX1 had advanced tumor stage, positive lymphatic vascular invasion, and a poor prognosis, while the silencing of PROX1 in GC cells led to inhibited cell migration, invasion, and proliferation [20]. The differential expression homeodomain-containing gene 10 (HOXC10) was found to be upregulated in GC tissues and associated with decreased recurrence-free survival based on TCGA database, and the overexpression of HOXC10 could promote the proliferation and migration of GC cells, indicating the prognostic value and therapeutic potency of HOXC10 in GC [21]. The aforementioned studies provide evidence for the key roles of DEGs in the prognosis and progression of GC. According to the

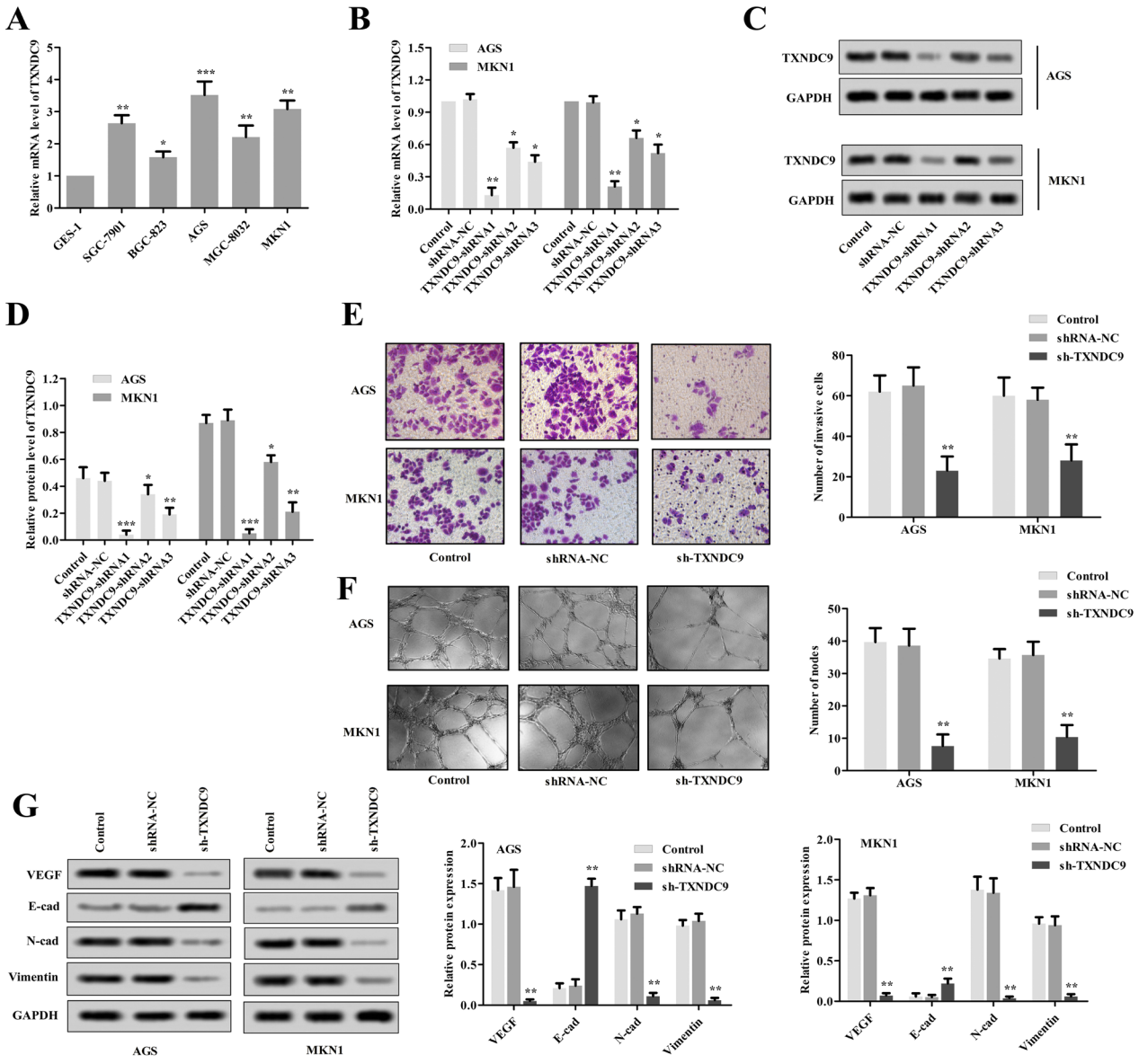

Figure 3. Effects of TXNDC9 on GC cell invasion and EMT. A) TXNDC9 mRNA expression was detected using qRT-PCR, and was found to be increased in GC cell lines compared with the normal cell line (*p<0.05, **p<0.01, ***p<0.001 vs. GES-1). B) Three shRNAs (shRNA1, shRNA2, and shRNA3) against TXNDC9 were transfected into AGS and MKN1 cells and the mRNA expression of TXNDC9 measured by qRT-PCR was inhibited by the shRNAs in both AGS and MKN1 cells (*p<0.05, **p<0.01 vs. control). C, D) The protein expression of TXNDC9 was measured using western blot assay, which was inhibited by TXNDC9-shRNAs (*p<0.05, **p<0.01, ***p<0.001 vs. control). E) The shRNA1 was selected to inhibit TXNDC9 expression in subsequent cell experiments, and the cell invasion of AGS and MKN1 cells analyzed by the Transwell assay was significantly decreased by the knockdown of TXNDC9 (p<0.01 vs. control). F) The number of nodes in microtubule formation analysis was decreased by the silencing of TXNDC9 (**p<0.01 vs. control). G) TXNDC9 knockdown suppressed the EMT processes in AGS and MKN1 cells, which was demonstrated by the decreased VEGF, N-cad, vimentin, and increased E-cad (**p<0.01 vs. control). Each experiment was repeated at least 3 times.**

expression data from TCGA database, this study found that TXNDC9 expression was dramatically elevated in GC tissues compared to normal controls, indicating that TXNDC9 might be involved in GC development and progression.

TXNDC9 has been described as an oncogene in the tumorigenesis in several carcinomas [10–12]. High TXNDC9 expression found in prostate cancer tissues was associated with an advanced clinical stage, and TXNDC9 overexpression led to enhanced carcinogenesis through regulating the activity of androgen receptor signaling that induced by reactive oxygen species [10]. In hepatocellular carcinoma, TXNDC9 directly targets MYC, leading to the regulation of MYC-mediated transcriptional activation, thereby promoting tumor cell proliferation [11]. The upregulation

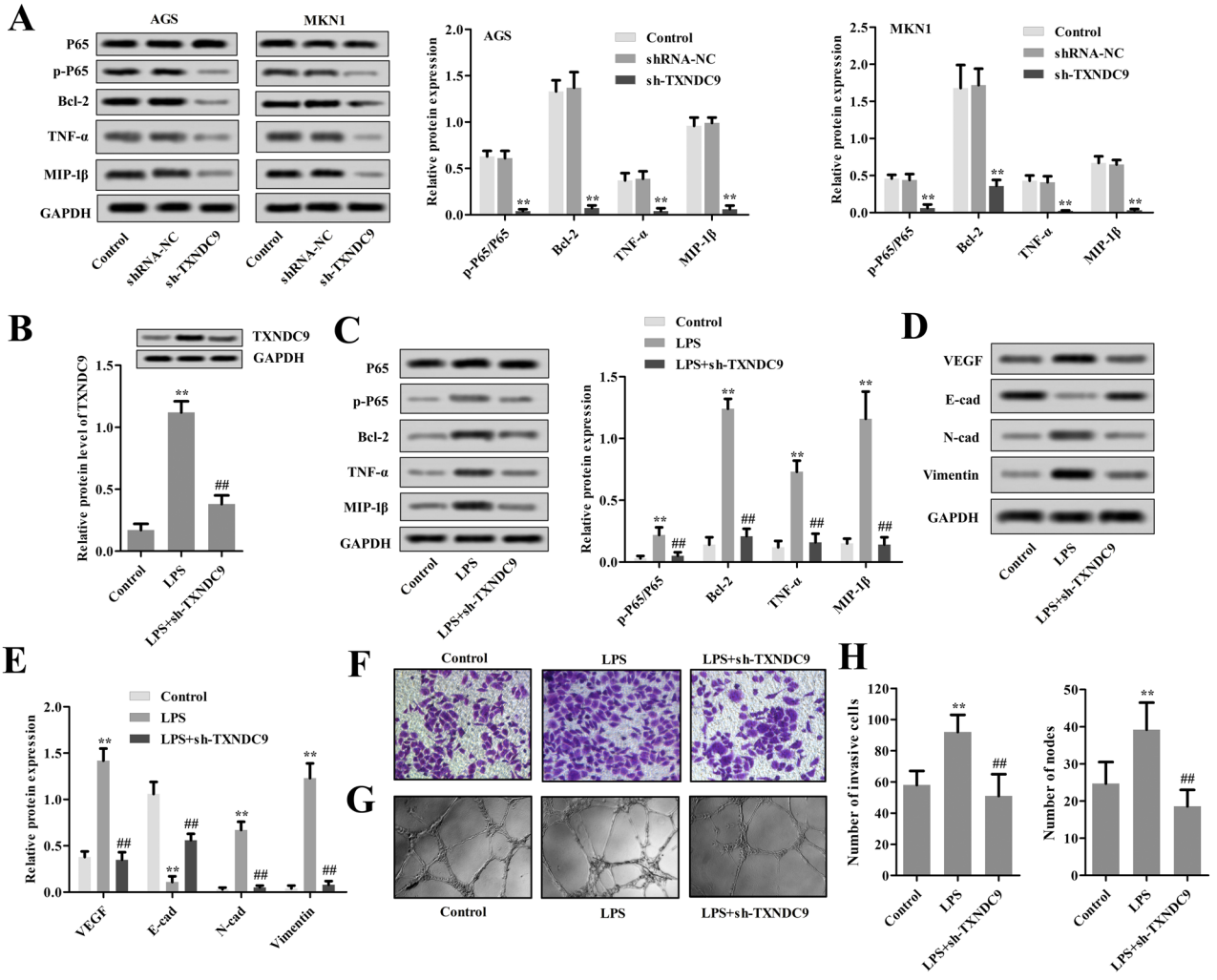

Figure 4. TXNDC9 silencing inhibits GC cell invasion and EMT through the NF-κB signaling pathway. A) The activity of the NF-κB signaling pathway was detected by detecting the ratio of p-P65/P65 and the levels of downstream protein (Bcl-2, TNF-α, and MIP-1β) by western blot assay, and activity of NF-κB signaling pathway was found to be inhibited by TXNDC9 reduction in both AGS and MKN1 cells (p<0.01 vs. control). B) LPS was used to activate the NF-κB signaling pathway, and a rescue experiment was performed by cell transfection of sh-TXNDC9 in AGS cells under LPS treatment. The protein expression of TXNDC detected by western blot was upregulated by LPS, but this upregulation in TXNDC was abolished by sh-TXNDC9 (**p<0.01 vs. control; ##p<0.01 vs. LPS). C) LPS induced activated NF-κB signaling pathway, which was manifested by detecting the ratio of p-P65/P65 and the levels of downstream protein (Bcl-2, TNF-α, and MIP-1β) by western blot assay, but this activation was reversed by TXNDC9 silencing (**p<0.01 vs. control; ##p<0.01 vs. LPS). D, E) By examining the protein levels of VEGF, E-cad, N-cad, and vimentin, the EMT processes of AGS were promoted by LPS, but this effect was reversed by TXNDC9 inhibition (**p<0.01 vs. control; ##p<0.01 vs. LPS). F–H) The invasion measured by Transwell assay and the tubule formation abilities of AGS cells were enhanced by LPS, but TXNDC9 knockdown abolished these effects of LPS (**p<0.01 vs. control; ##p<0.01 vs. LPS). Each experiment was repeated at least 3 times.**

of TXNDC9 was also observed in glioma, and the knockdown of TXNCD9 in glioma cells increased cell apoptosis and autophagy and promoted tumor cell differentiation by regulating p53 [12]. In colorectal carcinoma, oxaliplatin treatment led to enhanced expression of TXNDC9, and the manipulation of TXNDC9 significantly regulated oxaliplatin-induced tumor cell autophagy and apoptosis, indicating the potential of TXNDC9 as a target to counteract oxaliplatin resistance [10]. In addition, the clinical value of TXNDC9 was also previously investigated. Hepatocellular carcinoma patients with high TXNDC9 levels had significantly poor overall survival than those with low TXNDC9 levels [11]. Lu et al. reported that high expression of TXNDC9 was associated with poor prognosis in patients with colorectal carcinoma [13]. However, the role of TXNDC9 in GC remains unknown. This study found that TXNDC9 was highly expressed in GC tissues (TCGA) and cell lines, indicating the potential oncogenic role of TXNDC9 in GC. The survival information collected from TCGA database showed that high expression of TXNDC9 predicted a poor prognosis of

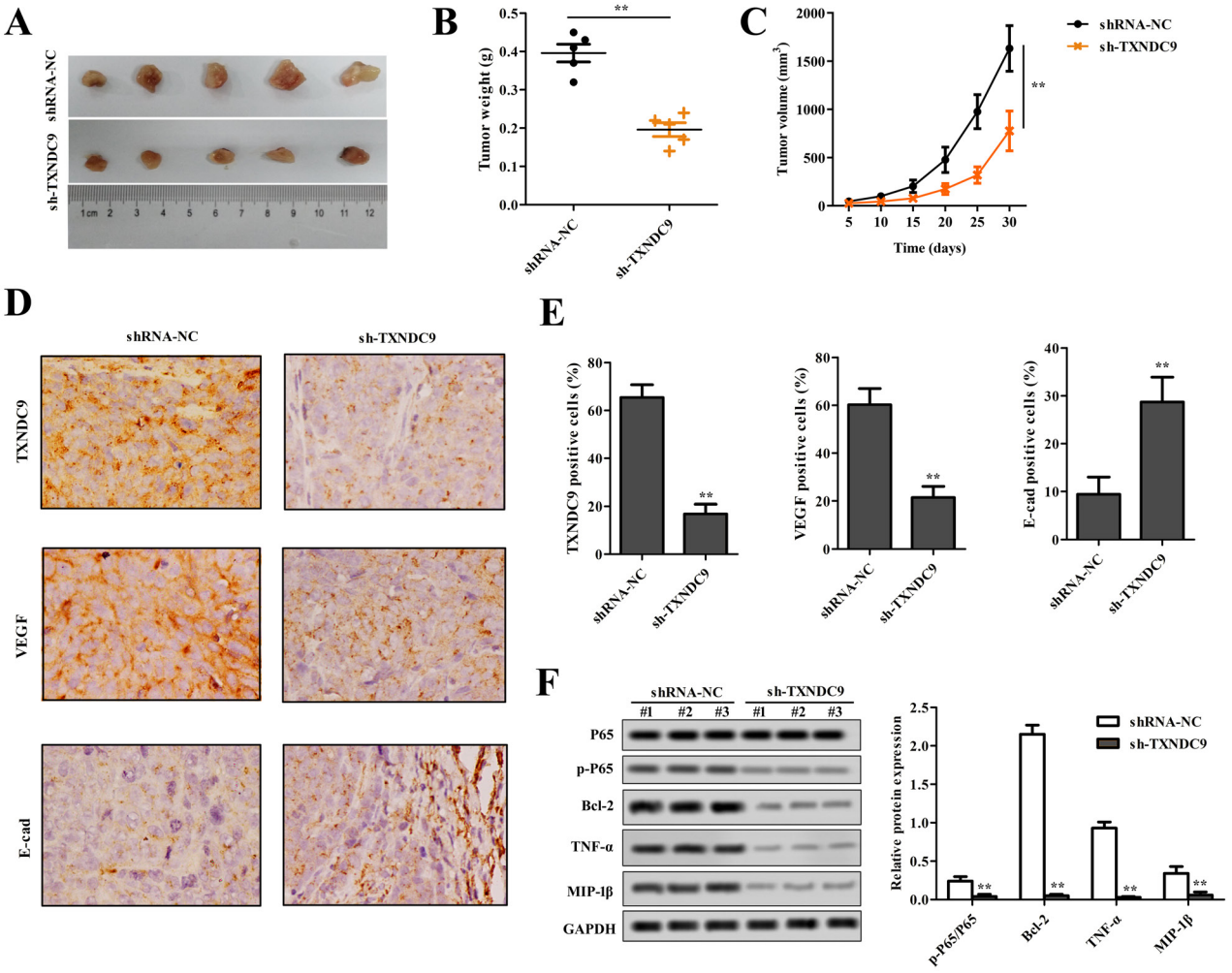

Figure 5. TXNDC9 inhibition suppressed tumorigenesis by *in vivo* experiments. A–C) Animal tumor models injected with AGS cells with shRNA-NC and sh-TXNDC9 were constructed, and the tumor weight and volume were inhibited by the TXNDC9 reduction *in vivo* (p<0.01 vs. shRNA-NC; 5 mice in each group). D, E) TXNDC9, VEGF, and E-cadherin protein levels were detected using IHC staining, and were significantly inhibited by TXNDC9-shRNA1 in the tumors (**p<0.01 vs. shRNA-NC). F) The activity of the NF-κB signaling pathway, which was detected by examining the ratio of p-P65/P65 and the levels of downstream protein (Bcl-2, TNF-α, and MIP-1β) by western blot assay, was inhibited by TXNDC9 reduction *in vivo* (**p<0.01 vs. shRNA-NC). Each experiment was repeated at least 3 times.**

GC, which was consistent with the survival analysis results in a previous publication regarding the role of TXNDC9 in hepatocellular carcinoma [11]. Furthermore, the *in vitro* and *in vivo* experiments explored the functional role of TXNDC9 in GC progression and confirmed the oncogenic role of TXNDC9, which manifested by the inhibited GC cell invasion, microtubule formation, EMT, and tumorigenesis induced by TXNDC9 silencing. Similar to the previous reports, this study also demonstrated the tumor-promoting action of TXNDC9 in GC. Of note, this study focused on the effects of TXNDC9 on GC cell metastatic potential, which was different from the previous studies that analyzed the regulation of cell proliferation by TXNDC9 [10–12]. Thus, the results of this study might contribute to further understanding the biological function of TXNDC9 in malignant tumors.

The NF-κB signaling pathway is an important pathway to mediate carcinogenesis in various human malignancies [16]. Some GC progression-related key genes exert biological function by regulating the activity of the NF-κB signaling pathway. For instance, Fan et al. demonstrated that fermitin family member 1 (FERMT1) predicted prognosis and promoted tumor progression through activating the NF-κB signaling in GC [22]. Zhang et al. have provided evidence for the differentially expressed zinc finger and BTB domain containing 20 (ZBTB20) in GC as an oncogene and indicated the mediating role of the NF-κB signaling pathway in the function of ZBTB20 [23]. Considering the regulatory function of TXNDC9 in the tumorigenesis of human cancers, this study suspected that there might be a relationship between the NF-κB signaling pathway and TXNDC9.

By downregulating TXNDC9 in both *in vivo* and *in vitro*, the phosphorylation levels of P65 and the expression of downstream proteins were significantly reduced, suggesting the inhibitory effects of TXNDC9 silencing on the activity of the NF-κB signaling pathway. However, the present study did not further explore the mechanisms in the regulation of TXNDC9 in the NF-κB signaling pathway, which was one of the limitations of this study. Further studies need to analyze the interaction between TXNDC9 and the NF-κB pathway by co-immunoprecipitation. In previously reported research, TXNDC9 has been demonstrated to behave as an effector for some transcription factors, such as MYC, p53, and Nrf2 [11, 12, 24]. The crosstalk of the transcription factors and NF-κB might be involved in the regulatory effects of TXNDC9 on the NF-κB signaling pathway, which needs to be analyzed and confirmed in future studies.

In addition, this study used LPS as an activator of the NF-κB signaling pathway to induce GC the activity of the NF-κB signaling and thereby enhancing tumor cell metastasis. LPS has been documented to promote metastasis processes in different cancer cell types, and the NF-κB signaling pathway is involved in the LPS-induced tumor cell migration [17]. In GC cells, the NF-κB signaling pathway was activated by LPS and subsequently led to aggressive behaviors [25]. Thus, this study performed a pathway recovery experiment using LPS treatment, which led to the activation of the NF-κB signaling pathway in GC cells. In GC cells with reduced TXNDC9, the enhanced cell invasive ability, EMT, and NF-κB signaling pathway activity were significantly reversed. LPS has been documented to activate the NF-κB signaling pathway through multiple pathways [26, 27]. This study found that LPS-induced active NF-κB signaling pathway was blocked by the reduction of TXNDC9. Considering the significantly increased TXNDC9 expression by LPS treatment, it is wondered that whether TXNDC9 played a role in the regulatory effects of LPS on the NF-κB signaling pathway. However, the analysis results of this study could not give a definitive verdict, and the relationship between TXNDC9, LPS, and LPS-affected NF-κB signaling pathway needed to be verified with further studies. Regarding the effects of TXNDC9 on the NF-κB signaling pathway, the *in vivo* analysis in this study also confirmed the changes in the NF-κB signaling pathway under the condition of TXNDC9 downregulation. Overall, these data indicated that TXNDC9 may promote the NF-κB-regulated metastatic potential in GC.

In conclusion, this study demonstrated that TXNDC9 was highly expressed in GC tissues and cell lines and had predictive value for the overall survival prognosis of GC. The *in vitro* and *in vivo* experiments demonstrated that the silencing of TXNDC9 inhibited GC cell invasion and EMT through inactivating the NF-κB signaling pathway. The results of this study may provide a novel prognostic biomarker and a candidate therapeutic target for GC. Although we provide evidence for the clinical role of TXNDC9, its prognostic performance needs to be confirmed in a large scale of validation population.

Supplementary information is available in the online version of the paper.

Acknowledgments: This study was funded by the National Natural Science Foundation of China (NO. 81502442).

References

[1] SMYTH EC, NILSSON M, GRABSCH HI, VAN GRIEKEN NC, LORDICK F. Gastric cancer. Lancet 2020; 396: 635–648. https://doi.org/10.1016/S0140-6736(20)31288-5

[2] ZHANG Y, YU J. The role of MRI in the diagnosis and treatment of gastric cancer. Diagn Interv Radiol 2020; 26: 176–182. https://doi.org/10.5152/dir.2019.19375

[3] JOHNSTON FM, BECKMAN M. Updates on Management of Gastric Cancer. Curr Oncol Rep 2019; 21: 67. https://doi.org/10.1007/s11912-019-0820-4

[4] MACHLOWSKA J, BAJ J, SITARZ M, MACIEJEWSKI R, SITARZ R. Gastric Cancer: Epidemiology, Risk Factors, Classification, Genomic Characteristics and Treatment Strategies. Int J Mol Sci 2020; 21. https://doi.org/10.3390/ijms21114012

[5] ZHANG J, LI X, HAN X, LIU R, FANG J. Targeting the Thioredoxin System for Cancer Therapy. Trends Pharmacol Sci 2017; 38: 794–808. https://doi.org/10.1016/j.tips.2017.06.001

[6] LEE D, XU IM, CHIU DK, LEIBOLD J, TSE AP et al. Induction of Oxidative Stress Through Inhibition of Thioredoxin Reductase 1 Is an Effective Therapeutic Approach for Hepatocellular Carcinoma. Hepatology 2019; 69: 1768–1786. https://doi.org/10.1002/hep.30467

[7] REN X, ZOU L, ZHANG X, BRANCO V, WANG J et al. Redox Signaling Mediated by Thioredoxin and Glutathione Systems in the Central Nervous System. Antioxid Redox Signal 2017; 27: 989–1010. https://doi.org/10.1089/ars.2016.6925

[8] HARRIS IS, TRELOAR AE, INOUE S, SASAKI M, GORRINI C et al. Glutathione and thioredoxin antioxidant pathways synergize to drive cancer initiation and progression. Cancer Cell 2015; 27: 211–222. https://doi.org/10.1016/j.ccell.2014.11.019

[9] MA F, HOU L, YANG L. Txndc9 Is Required for Meiotic Maturation of Mouse Oocytes. Biomed Res Int 2017; 2017: 6265890. https://doi.org/10.1155/2017/6265890

[10] LIU X, LIU B, LI R, WANG F, WANG N et al. miR-146a-5p Plays an Oncogenic Role in NSCLC via Suppression of TRAF6. Frontiers in cell and developmental biology 2020; 8: 847. https://doi.org/10.3389/fcell.2020.00847

[11] CHEN D, ZOU J, ZHAO Z, TANG X, DENG Z et al. TXNDC9 promotes hepatocellular carcinoma progression by positive regulation of MYC-mediated transcriptional network. Cell Death Dis 2018; 9: 1110. https://doi.org/10.1038/s41419-018-1150-4

[12] ZHENG T, CHEN K, ZHANG X, FENG H, SHI Y et al. Knockdown of TXNDC9 induces apoptosis and autophagy in glioma and mediates cell differentiation by p53 activation. Aging (Albany NY) 2020; 12: 18649–18659. https://doi.org/10.18632/aging.103915

[13] LU A, WANGPU X, HAN D, FENG H, ZHAO J et al. TXNDC9 expression in colorectal cancer cells and its influence on colorectal cancer prognosis. Cancer Invest 2012; 30: 721–726. https://doi.org/10.3109/07357907.2012.732160

[14] NIRANJAN R, NATH C, SHUKLA R. Guggulipid and nimesulide differentially regulated inflammatory genes mRNA expressions via inhibition of NF-kB and CHOP activation in LPS-stimulated rat astrocytoma cells, C6. Cell Mol Neurobiol 2011; 31: 755–764. https://doi.org/10.1007/s10571-011-9684-3

[15] ZHANG JX, CHEN ZH, XU Y, CHEN JW, WENG HW et al. Downregulation of MicroRNA-644a Promotes Esophageal Squamous Cell Carcinoma Aggressiveness and Stem Cell-like Phenotype via Dysregulation of PITX2. Clin Cancer Res 2017; 23: 298–310. https://doi.org/10.1158/1078-0432.CCR-16-0414

[16] SOKOLOVA O, NAUMANN M. NF-kappaB Signaling in Gastric Cancer. Toxins (Basel) 2017; 9. https://doi.org/10.3390/toxins9040119

[17] JAIN S, DASH P, MINZ AP, SATPATHI S, SAMAL AG et al. Lipopolysaccharide (LPS) enhances prostate cancer metastasis potentially through NF-kappaB activation and recurrent dexamethasone administration fails to suppress it in vivo. Prostate 2019; 79: 168–182. https://doi.org/10.1002/pros.23722

[18] YU C, CHEN J, MA J, ZANG L, DONG F et al. Identification of Key Genes and Signaling Pathways Associated with the Progression of Gastric Cancer. Pathol Oncol Res 2020; 26: 1903–1919. https://doi.org/10.1007/s12253-019-00781-3

[19] NIE K, SHI L, WEN Y, PAN J, LI P et al. Identification of hub genes correlated with the pathogenesis and prognosis of gastric cancer via bioinformatics methods. Minerva Med 2020; 111: 213–225. https://doi.org/10.23736/S0026-4806.19.06166-4

[20] UETA K, OTOWA Y, KAKEJI Y, HIRASHIMA M. PROX1 Is Associated with Cancer Progression and Prognosis in Gastric Cancer. Anticancer Res 2018; 38: 6139–6145. https://doi.org/10.21873/anticanres.12966

[21] KIM J, BAE DH, KIM JH, SONG KS, KIM YS et al. HOXC10 overexpression promotes cell proliferation and migration in gastric cancer. Oncol Rep 2019; 42: 202–212. https://doi.org/10.3892/or.2019.7164

[22] FAN H, ZHANG S, ZHANG Y, LIANG W, CAO B. FERMT1 promotes gastric cancer progression by activating the NF-kappaB pathway and predicts poor prognosis. Cancer Biol Ther 2020; 21: 815–825. https://doi.org/10.1080/15384047.2020.1792218

[23] ZHANG Y, ZHOU X, ZHANG M, CHENG L, ZHANG Y et al. ZBTB20 promotes cell migration and invasion of gastric cancer by inhibiting IkappaBalpha to induce NF-kappaB activation. Artif Cells Nanomed Biotechnol 2019; 47: 3862–3872. https://doi.org/10.1080/21691401.2019.1670188

[24] ZHOU W, FANG C, ZHANG L, WANG Q, LI D et al. Thioredoxin domain-containing protein 9 (TXNDC9) contributes to oxaliplatin resistance through regulation of autophagy-apoptosis in colorectal adenocarcinoma. Biochem Biophys Res Commun 2020; 524: 582–588. https://doi.org/10.1016/j.bbrc.2020.01.092

[25] LI H, XIA JQ, ZHU FS, XI ZH, PAN CY et al. LPS promotes the expression of PD-L1 in gastric cancer cells through NF-kappaB activation. J Cell Biochem 2018; 119: 9997–10004. https://doi.org/10.1002/jcb.27329

[26] WANG L, WU J, GUO X, HUANG X, HUANG Q. RAGE Plays a Role in LPS-Induced NF-kappaB Activation and Endothelial Hyperpermeability. Sensors (Basel) 2017; 17. https://doi.org/10.3390/s17040722

[27] WAN J, SHAN Y, FAN Y, FAN C, CHEN S et al. NF-kappaB inhibition attenuates LPS-induced TLR4 activation in monocyte cells. Mol Med Rep 2016; 14: 4505–4510. https://doi.org/10.3892/mmr.2016.5825

https://doi.org/10.4149/neo_2021_210806N1115

High level of TXNDC9 predicts poor prognosis and contributes to the NF-κB-regulated metastatic potential in gastric cancer

Qun-Cao YANG, Nan HAO, Rui-Hua LI, Yuan-Yuan DUAN, Yong ZHANG*

Supplementary Information

Supp. 1 Clinical information of the 375 GC patients collected from TCGA database.

	character	TCGA dataset (n=375)
Status	Alive	228
	Dead	147
Age	Mean (SD)	65.8 (10.7)
	Median [MIN, MAX]	67 [35,90]
Gender	FEMALE	134
	MALE	241
Race	ASIAN	74
	BLACK	11
	ISLANDER	1
	WHITE	238
pT_stage	T1	5
	T1a	2
	T1b	12
	T2	58
	T2a	9
	T2b	13
	T3	168
	T4	30
	T4a	46

	T4b	24
	TX	8
pN_stage	N0	111
	N1	97
	N2	75
	N3	26
	N3a	42
	N3b	6
	NX	16
pM_stage	M0	330
	M1	25
	MX	20
pTNM_stage	I	2
	IA	14
	IB	37
	II	27
	IIA	35
	IIB	49
	III	3
	IIIA	60
	IIIB	52
	IIIC	35

	IV	38
Grade	G1	10
	G2	137
	G3	219
	GX	9

Supp. 2 Expression of TXNDC9, BCL2 and VEGFA and the clinicopathological features of GC patients used for Cox regression analysis.

	time	status	VEGFA	BCL2	TXNDC9	Age	Gender	Race	pT_stage	pN_stage
TCGA-3M-AB46-01	1765	0	4.923461289	0.765930786	3.854806412	70	M	WHITE	T2	N0
TCGA-B7-5818-01	356	0	6.177160917	2.023320509	4.315056705	62	M	WHITE	T2	N0
TCGA-B7-A5TI-01	595	0	5.351827517	1.838150613	4.644994366	52	M	WHITE	T4	N3
TCGA-BR-4253-01	124	1	5.662471466	2.561636847	5.496504826	80	F	WHITE	T3	N1
TCGA-BR-4267-01	188	1	5.162666768	1.491431769	5.057383583	51	M	WHITE	T2	N0
TCGA-BR-4279-01	291	1	3.62516551	3.097024142	5.662101364	43	M	WHITE	T2	N1
TCGA-BR-4280-01	201	1	5.011818126	2.615880379	4.490226808	78	F	WHITE	T2	N1
TCGA-BR-4361-01	0	0	4.741150241	2.760751781	4.823197662	66	F	WHITE	T4	N0
TCGA-BR-4368-01	0	0	4.674214839	3.194867673	4.31651922	78	F	WHITE	T4	N2
TCGA-BR-6452-01	1055	0	5.134257991	2.514780381	4.538480508	78	F	WHITE	T3	N0
TCGA-BR-6453-01	485	0	2.967592226	3.353225573	3.984071493	54	M	WHITE	T2	N1
TCGA-BR-6454-01	0	0	5.379303396	2.67820496	4.73592731	58	M	WHITE	T3	N0
TCGA-BR-6455-01	422	1	5.421474619	2.283527916	4.80862684	59	M	WHITE	T3	N1

TCGA-BR-6456-01	526	1	5.958550691	3.030668608	5.296734924	74	F	WHITE	T3	N1
TCGA-BR-6457-01	416	0	4.551571367	3.230082558	4.131248635	69	M	WHITE	T3	N0
TCGA-BR-6458-01	588	1	5.174079412	2.720949463	5.597358335	57	F	WHITE	T3	N1
TCGA-BR-6563-01	1190	0	3.1624962	3.313342826	3.996574883	60	M	WHITE	T3	N1
TCGA-BR-6564-01	794	1	3.687107774	3.584640198	4.307254105	46	F	WHITE	T3	N2
TCGA-BR-6565-01	279	1	5.51611021	3.042400741	5.364878514	67	M	WHITE	T4	N0
TCGA-BR-6566-01	997	0	3.625109068	1.945911281	4.368712831	64	F	WHITE	T3	N0
TCGA-BR-6705-01	779	1	4.438261392	3.319501477	4.37034708	68	F	WHITE	T3	N3
TCGA-BR-6707-01	491	0	6.123045939	1.635202916	4.450355186	75	M	WHITE	T3	N0
TCGA-BR-6709-01	370	1	4.217629912	3.319722052	5.073906247	57	F	WHITE	T3	N3
TCGA-BR-6710-01	273	0	4.789886792	1.644549243	3.803901713	41	M	WHITE	T2	N0
TCGA-BR-6801-01	1223	0	4.224015727	1.231230933	4.103334349	70	M	WHITE	T3	N0
TCGA-BR-6802-01	940	0	4.922497548	1.987123506	4.458096081	65	M	WHITE	T3	N2
TCGA-BR-6803-01	949	0	4.540061021	3.295099916	4.269542076	54	F	WHITE	T3	N0
TCGA-BR-6852-01	1367	0	5.468129925	2.49494584	3.92664836	64	F	WHITE	T3	N0
TCGA-BR-7196-01	666	0	5.753180612	3.232085181	4.706079127	64	M	WHITE	T3	N3
TCGA-BR-7197-01	280	0	5.226584364	2.075930576	4.857011875	69	M	WHITE	T3	N0
TCGA-BR-7704-01	1072	0	5.652023824	1.724490534	4.58680658	69	F	WHITE	T3	N0
TCGA-BR-7707-01	1090	0	5.173699085	2.0345319	4.227662428	69	F	WHITE	T2	N0
TCGA-BR-7715-01	1023	0	5.467873845	2.359322342	4.835197833	65	M	WHITE	T3	N0
TCGA-BR-7716-01	1210	0	4.736773073	2.700855566	4.995068904	62	F	WHITE	T3	N1
TCGA-BR-7717-01	552	1	3.954098676	1.481616123	4.543812832	63	M	WHITE	T4	N1

TCGA-BR-7722-01	466	1	5.53468446	1.836264081	3.863450781	62	M	WHITE	T3	N1
TCGA-BR-7723-01	874	1	5.573045058	3.249996355	4.677694058	59	M	WHITE	T3	N3
TCGA-BR-7901-01	105	1	6.320454581	2.603073176	4.846759992	74	M	WHITE	T3	N1
TCGA-BR-7957-01	276	1	4.064625664	3.431623801	5.070288137	50	F	WHITE	T3	N3
TCGA-BR-7958-01	899	0	5.519215625	2.802178532	4.600312039	60	M	WHITE	T4	N0
TCGA-BR-7959-01	1010	0	4.580177189	3.391982464	4.747866225	59	M	WHITE	T4	N1
TCGA-BR-8058-01	1133	0	4.444186842	3.566161316	4.894017963	53	F	WHITE	T4	N2
TCGA-BR-8059-01	439	1	4.754929449	2.103651141	4.497361487	72	M	WHITE	T4	N1
TCGA-BR-8060-01	348	1	4.146293485	3.187022987	5.015781409	75	F	WHITE	T2	N2
TCGA-BR-8077-01	21	0	4.52775208	1.723842152	4.483921915	58	F	WHITE	T4	N1
TCGA-BR-8080-01	292	1	4.060311273	3.584759179	4.711175015	72	F	WHITE	T4	N3
TCGA-BR-8081-01	981	0	4.268091483	3.202067555	4.115698511	71	F	WHITE	T4	N0
TCGA-BR-8284-01	245	1	5.268385395	3.320400927	4.814542667	72	F	WHITE	T4	N3
TCGA-BR-8286-01	895	0	4.884216488	2.375598371	4.938079256	49	M	WHITE	T3	N0
TCGA-BR-8289-01	81	1	3.966087066	1.877085034	5.144522113	57	M	WHITE	T4	N3
TCGA-BR-8291-01	607	1	5.342880203	3.105411557	4.559440207	61	M	WHITE	T3	N1
TCGA-BR-8295-01	67	1	4.008476316	2.328410726	4.522026262	60	F	WHITE	T4	N0
TCGA-BR-8296-01	474	1	5.144687149	3.286646472	4.803131871	58	F	WHITE	T4	N2
TCGA-BR-8297-01	225	0	3.933822333	3.402172799	4.806330443	58	M	WHITE	T4	N3
TCGA-BR-8361-01	946	0	5.330530613	2.55516776	4.162946286	71	F	WHITE	T4	N2
TCGA-BR-8364-01	675	0	4.277585371	3.864519032	4.768260725	42	F	WHITE	T4	N2
TCGA-BR-8365-01	533	1	4.0751656	4.233440463	4.351782882	70	F	WHITE	T3	N0

TCGA-BR-8366-01	29	0	3.945079305	3.085390265	5.353941274	80	F	WHITE	T3	N0
TCGA-BR-8367-01	801	1	4.330428993	3.693811434	4.863131873	55	M	WHITE	T3	N3
TCGA-BR-8368-01	131	0	4.678103293	2.690626667	4.457487647	84	F	WHITE	T2	N0
TCGA-BR-8369-01	427	0	4.223961303	2.883266191	4.765131387	76	F	WHITE	T3	N3
TCGA-BR-8371-01	359	1	2.975616606	3.845899252	4.013449182	62	M	WHITE	T3	N3
TCGA-BR-8372-01	951	0	4.785987734	3.138982356	5.149986437	63	M	WHITE	T4	N3
TCGA-BR-8373-01	450	0	6.291317221	2.620716608	5.037895889	65	F	WHITE	T4	N1
TCGA-BR-8380-01	21	0	3.436478208	4.066351908	4.351652701	55	M	WHITE	T4	N3
TCGA-BR-8381-01	224	0	4.855281532	2.874912217	4.509835661	51	M	WHITE	T3	N1
TCGA-BR-8382-01	762	1	4.262215024	2.218481964	3.808016255	67	F	WHITE	T4	N3
TCGA-BR-8384-01	113	0	4.197095805	4.52450099	4.281272039	69	M	WHITE	T4	N2
TCGA-BR-8483-01	164	0	4.748386646	1.194864909	4.725008958	59	M	WHITE	T3	N2
TCGA-BR-8484-01	766	1	5.619790497	2.782039813	4.372710637	61	M	WHITE	T4	N1
TCGA-BR-8485-01	280	0	5.236747078	3.334567392	5.363638022	68	F	WHITE	T4	N3
TCGA-BR-8486-01	615	0	7.453355686	2.675758797	4.608613594	90	F	WHITE	T1	N0
TCGA-BR-8487-01	34	0	5.987913391	0.863098343	3.764949246	64	F	WHITE	T3	N0
TCGA-BR-8588-01	389	0	4.426124137	2.620737701	4.706775921	55	F	WHITE	T4	N0
TCGA-BR-8589-01	825	0	5.14994813	2.161051236	5.257965015	56	M	WHITE	T4	N1
TCGA-BR-8590-01	284	1	3.579404963	3.413720014	4.953630567	62	M	WHITE	T4	N2
TCGA-BR-8591-01	856	0	5.94115502	2.768795027	4.114829021	79	M	WHITE	T4	N3
TCGA-BR-8592-01	191	1	3.488732375	4.40636544	4.427444657	63	F	WHITE	T4	N1
TCGA-BR-8676-01	229	0	3.529156211	1.358622896	4.412508712	59	M	WHITE	T3	N3

TCGA-BR-8677-01	813	0	5.247098164	2.940652872	4.973575988	74	F	WHITE	T3	N3
TCGA-BR-8678-01	754	0	5.604089277	4.37468935	5.704765456	76	M	WHITE	T2	N0
TCGA-BR-8679-01	0	0	5.078558784	2.283031475	5.591657417	63	F	WHITE	T2	N0
TCGA-BR-8680-01	972	0	6.408484476	1.887992717	5.091121403	45	M	ASIAN	T4	N2
TCGA-BR-8682-01	991	0	4.51539794	3.432525284	4.403547383	52	M	ASIAN	T4	N0
TCGA-BR-8683-01	300	1	8.733533487	3.211279032	5.228920598	75	M	ASIAN	T4	N2
TCGA-BR-8686-01	635	1	7.157016919	3.420891451	4.738916846	69	M	ASIAN	T4	N1
TCGA-BR-8687-01	250	1	4.48100595	1.796883102	4.340962673	67	F	WHITE	T4	N2
TCGA-BR-8690-01	325	0	4.547278467	1.594565168	4.2883898	54	F	WHITE	T3	N3
TCGA-BR-A44T-01	1038	0	3.075126702	3.798337804	4.226717528	53	F	WHITE	T3	N0
TCGA-BR-A44U-01	422	1	4.097258607	1.058371356	4.278615253	70	M	WHITE	T3	N3
TCGA-BR-A4CR-01	0	0	5.245332102	4.529905864	5.118853684	70	F	WHITE	T4	N3
TCGA-BR-A4CS-01	45	1	5.186849405	0.841776868	4.6654606	77	M	WHITE	T4	N3
TCGA-BR-A4IV-01	869	1	3.901165247	2.920332412	4.509389459	47	M	ASIAN	T4	N2
TCGA-BR-A4J4-01	16	0	4.703030877	4.036162037	5.035200094	39	M	ASIAN	T4	N2
TCGA-BR-A4J5-01	862	0	3.625909841	2.188402505	4.678723834	56	M	ASIAN	T4	N1
TCGA-BR-A4J6-01	20	0	3.988804914	1.542803383	4.846680432	69	F	WHITE	T3	N0
TCGA-BR-A4J8-01	411	0	4.914261721	2.207277492	4.046352569	71	F	WHITE	T3	N3
TCGA-BR-A4J9-01	14	0	2.771611449	3.459538064	4.009766176	55	M	WHITE	T3	N0
TCGA-BR-A4PF-01	35	0	4.115182824	2.897727158	5.292978267	72	M	WHITE	T4	N2

TCGA-BR-A4QL-01	491	1	3.807458284	2.023869746	3.058163424	75	F	WHITE	T3	N3
TCGA-CD-5798-01	408	0	3.575360415	2.626242479	4.924478926	82	M	ASIAN	T3	N0
TCGA-CD-5799-01	396	0	5.054913817	0.809629626	4.542401374	45	M	ASIAN	T2	N1
TCGA-CD-5800-01	400	0	5.470591879	1.438173246	4.446431952	51	F	ASIAN	T3	N0
TCGA-CD-5801-01	401	1	4.439493054	1.630562355	4.77207999	69	M	ASIAN	T3	N1
TCGA-CD-5803-01	341	1	4.621320929	3.986562643	4.871751656	78	F	ASIAN	T3	N0
TCGA-CD-5804-01	368	0	4.498369525	1.791699849	3.983793011	90	M	ASIAN	T3	N1
TCGA-CD-5813-01	377	1	3.790717285	3.311555127	4.02651606	60	M	ASIAN	T3	N0
TCGA-CD-8524-01	388	0	4.512188736	2.010102188	5.250201207	61	F	ASIAN	T3	N0
TCGA-CD-8525-01	383	0	4.04036417	1.116619202	4.343476912	82	F	ASIAN	T3	N1
TCGA-CD-8526-01	381	0	4.754919386	2.078548042	4.986989507	73	F	ASIAN	T3	N1
TCGA-CD-8527-01	218	1	4.171067958	0.793456219	4.603527036	72	F	ASIAN	T2	N1
TCGA-CD-8528-01	375	0	4.320520586	2.440516675	4.912656566	43	F	ASIAN	T4	N0
TCGA-CD-8529-01	374	0	5.340721607	3.13769091	4.292593563	65	M	ASIAN	T4	N0
TCGA-CD-8530-01	377	0	4.050510119	2.538343337	4.57653531	51	M	ASIAN	T3	N0
TCGA-CD-8531-01	383	0	2.018075389	3.717427096	5.296845427	66	F	ASIAN	T3	N1
TCGA-CD-8532-01	354	1	4.98957956	2.791830036	4.679962133	52	M	ASIAN	T3	N0
TCGA-CD-8533-01	468	0	3.662389525	3.028736117	4.895385953	48	M	ASIAN	T3	N0
TCGA-CD-8534-01	367	0	3.384087498	2.009111144	3.696289716	41	M	ASIAN	T3	N0
TCGA-CD-8535-01	390	0	5.687320685	3.752943463	5.013295397	59	M	ASIAN	T3	N1
TCGA-CD-A486-01	192	1	7.28835646	0.948237716	4.606833753	68	M	ASIAN	T3	N0

TCGA-CD-A487-01	374	0	3.870703201	1.585389026	4.561414507	51	M	ASIAN	T3	N1
TCGA-CD-A489-01	344	1	3.676597116	3.119149637	5.196101381	58	M	ASIAN	T3	N0
TCGA-CD-A48A-01	378	0	4.283059889	1.579133644	4.429592429	57	M	ASIAN	T3	N0
TCGA-CD-A48C-01	353	1	4.293335044	1.170912694	4.740184709	79	F	ASIAN	T3	N1
TCGA-CD-A4MG-01	200	1	4.021804115	2.152755742	3.848849931	76	M	ASIAN	T3	N0
TCGA-CD-A4MH-01	371	0	5.144266191	1.953606984	4.246089974	86	F	ASIAN	T3	N0
TCGA-D7-5577-01	782	1	4.901461962	1.845113245	4.978460287	53	F	WHITE	T2	N3
TCGA-D7-5578-01	385	0	4.679405696	2.484075516	4.137379149	80	M	WHITE	T3	N2
TCGA-D7-6519-01	625	0	3.411701615	1.519816793	5.334859374	64	F	WHITE	T2	N1
TCGA-D7-6520-01	573	0	5.102421555	1.587855863	4.710281989	53	M	WHITE	T2	N2
TCGA-D7-6521-01	564	0	4.803402784	2.794376608	4.204469875	65	M	WHITE	T2	N2
TCGA-D7-6522-01	566	0	2.922139055	3.56814605	4.034708084	58	M	WHITE	T2	N0
TCGA-D7-6524-01	543	0	4.554018838	2.477608901	4.88840024	53	M	WHITE	T2	N1
TCGA-D7-6525-01	406	1	5.773030885	2.073054039	4.92087982	58	M	WHITE	T2	N2
TCGA-D7-6526-01	523	0	4.959606592	1.024986873	4.708648196	67	F	WHITE	T3	N2
TCGA-D7-6527-01	312	1	4.61732896	1.029362431	4.469575293	62	M	WHITE	T2	N1
TCGA-D7-6528-01	463	0	7.213195178	1.981220727	5.528469106	70	F	WHITE	T2	N0
TCGA-D7-6815-01	486	0	4.888651237	1.718839918	4.881684381	70	F	WHITE	T2	N2
TCGA-D7-6818-01	376	1	4.447995776	2.045954269	4.194701452	53	M	WHITE	T2	N3

TCGA-D7-6822-01	375	0	4.769287957	2.304060117	5.160821926	77	M	WHITE	T2	N0
TCGA-D7-8570-01	752	0	4.940436956	2.215436094	4.27154888	44	M	WHITE	T3	N3
TCGA-D7-8572-01	511	0	5.207879333	2.902209992	4.949981909	57	M	WHITE	T2	N2
TCGA-D7-8573-01	593	0	5.331160086	1.786768514	4.935645129	57	M	WHITE	T3	N0
TCGA-D7-8574-01	523	0	3.186452375	4.850057857	4.193743376	72	M	WHITE	T2	N3
TCGA-D7-8575-01	554	1	4.914762631	3.03226582	5.156666562	75	M	WHITE	T3	N2
TCGA-D7-8576-01	446	1	4.978705137	1.711687665	4.860933328	54	F	WHITE	T3	N3
TCGA-D7-8578-01	643	0	5.104653885	2.582457376	4.696541771	72	M	WHITE	T2	N0
TCGA-D7-8579-01	636	0	3.511992524	3.347651735	4.492279557	66	F	WHITE	T2	N2
TCGA-D7-A4YU-01	500	0	5.581700944	3.79302866	5.217167736	73	M	WHITE	T3	N3
TCGA-D7-A4YX-01	1108	0	6.133204806	2.278160918	4.984017378	63	M	WHITE	T3	N1
TCGA-D7-A4Z0-01	449	0	4.138223365	2.420501282	4.706973919	60	F	WHITE	T2	N2
TCGA-D7-A6EV-01	342	0	5.899912711	1.2670585	5.570194693	71	F	WHITE	T2	N2
TCGA-D7-A6EX-01	344	0	3.906389216	2.111718135	5.217329368	72	F	WHITE	T3	N2
TCGA-D7-A6EY-01	348	1	4.138672731	2.966398985	4.196565136	72	F	WHITE	T3	N3
TCGA-D7-A6EZ-01	618	1	7.457967376	2.02919575	5.578399386	66	M	WHITE	T3	N2
TCGA-D7-A6F0-01	678	0	6.100732768	1.89868217	4.871743445	79	F	WHITE	T2	N0
TCGA-D7-A6F2-01	476	0	4.095404256	2.109336421	4.622138704	62	M	WHITE	T2	N0
TCGA-D7-A747-01	255	1	2.87346369	3.339837763	4.321571756	57	M	WHITE	T3	N1
TCGA-D7-A748-01	132	1	3.835622234	2.201448287	4.641066009	41	F	WHITE	T4	N3

TCGA-D7-A74A-01	607	0	4.652075664	1.083162484	5.218134971	61	F	WHITE	T3	N2
TCGA-EQ-8122-01	243	1	5.69073639	1.617126008	5.549499878	71	F	WHITE	T3	N1
TCGA-F1-6177-01	200	0	6.873152641	3.219465382	3.652581406	90	M	BLACK	T1	N1
TCGA-F1-6874-01	440	0	5.816416138	3.402437297	4.238428107	79	M	WHITE	T2	N0
TCGA-F1-6875-01	2197	1	5.075348544	2.740308065	4.991507738	79	M	BLACK	T2	N0
TCGA-F1-A448-01	647	0	4.847815432	2.399343933	4.370346852	70	M	WHITE	T3	N3
TCGA-F1-A72C-01	346	0	4.565086099	1.639793719	5.311609428	68	M	ASIAN	T3	N0
TCGA-FP-7735-01	106	1	5.265630461	1.769920479	4.839479966	77	M	BLACK	T2	N0
TCGA-FP-7829-01	594	0	6.176671202	1.517650222	5.317091921	69	M	WHITE	T3	N1
TCGA-FP-7916-01	428	1	5.297428625	3.589098575	4.911375906	77	M	ASIAN	T4	N3
TCGA-FP-7998-01	678	0	5.580882565	3.755136973	4.479159786	77	M	WHITE	T4	N3
TCGA-FP-8099-01	519	0	7.322175422	2.095358617	4.937488764	79	M	WHITE	T3	N0
TCGA-FP-8209-01	1811	1	4.115376497	4.927737827	4.26897114	49	M	WHITE	T2	N0
TCGA-FP-8210-01	153	1	3.822756908	4.215106399	4.774569561	48	M	ASIAN	T3	N1
TCGA-FP-8211-01	413	0	4.771280617	1.455434268	4.548302475	62	M	WHITE	T3	N1
TCGA-FP-8631-01	17	0	6.807323434	1.315610558	4.66658963	68	M	WHITE	T3	N2
TCGA-FP-A4BF-01	168	1	4.448145414	2.43417571	5.399348845	68	M	WHITE	T3	N2
TCGA-FP-A8CX-01	7	0	4.517529144	1.646201063	4.482682138	60	M	WHITE	T4	N3
TCGA-FP-A9TM-01	189	0	4.231588672	3.363416204	4.830633627	77	M	WHITE	T1	N1
TCGA-HJ-7597-01	805	1	6.313797388	2.162749294	4.35512843	71	F	WHITE	T2	N0
TCGA-HU-8244-01	742	0	3.120484697	1.533070765	4.057383108	77	F	ASIAN	T1	N0

TCGA-HU-8249-01	881	0	5.414785233	1.845265755	5.496068901	76	M	ASIAN	T3	N2
TCGA-HU-8602-01	679	0	5.471691021	4.055904395	4.37579581	58	F	ASIAN	T4	N0
TCGA-HU-8604-01	694	0	4.920468412	2.948454895	4.883428613	82	F	ASIAN	T3	N0
TCGA-HU-8608-01	641	0	6.260289749	3.343821262	5.264379023	70	M	ASIAN	T4	N2
TCGA-HU-8610-01	23	0	5.613011408	2.72884336	5.429935249	75	M	ASIAN	T1	N0
TCGA-HU-A4G2-01	739	0	4.949086313	1.984115278	5.298093351	45	M	ASIAN	T3	N1
TCGA-HU-A4G3-01	170	0	3.53777075	1.549952531	4.327142825	54	M	ASIAN	T2	N2
TCGA-HU-A4G8-01	690	0	6.530135148	2.421676483	4.319094604	71	F	ASIAN	T3	N1
TCGA-HU-A4G9-01	736	0	4.037693791	1.158649099	3.646630855	67	F	ASIAN	T1	N0
TCGA-HU-A4GC-01	99	0	4.001896257	1.37658403	5.116807668	74	M	ASIAN	T4	N2
TCGA-HU-A4GD-01	692	0	4.115359272	1.190411728	5.46335106	56	M	ASIAN	T3	N1
TCGA-HU-A4GF-01	785	0	5.509247194	1.819522675	4.68757816	69	M	ASIAN	T3	N0
TCGA-HU-A4GH-01	358	0	4.462891354	0.919077087	5.054482548	75	M	ASIAN	T1	N0
TCGA-HU-A4GJ-01	650	0	3.02091991	4.389610547	4.235650737	60	F	ASIAN	T4	N3

TCGA-HU-A4GP-01	273	0	3.982024405	1.258934635	4.950067298	62	F	ASIAN	T2	N1
TCGA-HU-A4GQ-01	3	1	3.454398032	2.578907522	4.173882683	71	M	ASIAN	T4	N2
TCGA-HU-A4GT-01	198	0	4.055485653	2.352950112	4.190336994	71	F	ASIAN	T3	N0
TCGA-HU-A4GU-01	200	0	5.21177529	2.623252628	5.382173705	73	M	ASIAN	T3	N1
TCGA-HU-A4GX-01	616	0	4.335409188	1.987212425	4.133967775	70	F	ASIAN	T4	N2
TCGA-HU-A4GY-01	8	0	4.094641378	4.054923866	4.450499383	76	F	ASIAN	T4	N1
TCGA-HU-A4H0-01	64	0	5.972835595	2.177823629	5.692743985	72	M	ASIAN	T4	N3
TCGA-HU-A4H2-01	394	0	3.750867727	1.148304223	4.986166602	58	F	ASIAN	T3	N3
TCGA-HU-A4H3-01	882	0	6.634096209	2.171239707	4.444777458	56	F	ASIAN	T4	N3
TCGA-HU-A4H4-01	725	0	4.95109547	1.905603768	5.049275698	53	F	ASIAN	T2	N2
TCGA-HU-A4H5-01	724	0	6.899128872	1.706652767	5.603866061	71	M	ASIAN	T2	N0

TCGA-HU-A4H6-01	644	0	4.090619346	1.690344964	4.499462073	72	F	ASIAN	T3	N2
TCGA-HU-A4H8-01	428	0	4.288759754	1.398949416	4.362999146	77	M	ASIAN	T1	N1
TCGA-HU-A4HB-01	477	1	4.012239574	3.323072145	4.57812454	68	M	ASIAN	T2	N2
TCGA-HU-A4HD-01	1016	0	4.506769262	1.163635499	4.297641843	73	M	ASIAN	T3	N2
TCGA-IN-7806-01	1106	0	5.447227388	3.170143373	4.59015822	50	M	WHITE	T3	N1
TCGA-IN-7808-01	105	1	3.766716051	4.061326684	4.482020317	59	M	WHITE	T3	N3
TCGA-IN-8462-01	572	0	4.076531147	1.396704734	4.158513749	80	M	WHITE	T2	N1
TCGA-IN-8663-01	103	1	6.186378259	1.763165714	5.982053948	68	M	WHITE	T2	N2
TCGA-IN-A6RI-01	559	0	4.723757028	0.55719136	5.11333377	45	M	WHITE	T1	N0
TCGA-IN-A6RJ-01	379	0	4.256334898	0.952030634	4.269736413	64	M	WHITE	T1	N0
TCGA-IN-A6RL-01	406	1	5.595701845	1.64577012	4.568286032	84	M	WHITE	T2	N1
TCGA-IN-A6RN-01	594	0	6.500609719	0.893076369	4.519624374	72	F	WHITE	T1	N2
TCGA-IN-A6RR-01	205	1	5.59110519	1.358198377	5.09451354	84	M	WHITE	T3	N1
TCGA-IN-A6RS-01	383	0	6.95727831	1.71915351	5.780260015	76	M	WHITE	T1	N0
TCGA-IN-A7NR-01	198	0	3.652930107	1.713828832	4.581812102	64	F	WHITE	T3	N3
TCGA-IN-A7NT-01	323	0	4.60994741	1.088511995	5.967709879	73	F	WHITE	T3	N1
TCGA-IN-A7NU-01	356	0	3.325468726	1.434560688	5.459526619	69	M	WHITE	T3	N3
TCGA-IN-AB1V-01	479	0	3.9693326	2.365277972	4.47921844	63	M	WHITE	T1	N0

TCGA-IN-AB1X-01	411	0	5.853160989	2.592938866	5.217729233	78	F	WHITE	T3	N0
TCGA-IP-7968-01	77	0	6.357735569	2.504541835	4.893018676	74	M	WHITE	T3	N2
TCGA-KB-A93G-01	613	0	6.209931414	2.474949014	4.811275257	68	M	WHITE	T2	N0
TCGA-KB-A93H-01	1145	0	5.41585922	1.554518815	4.601406528	79	F	ASIAN	T3	N1
TCGA-KB-A93J-01	1124	0	4.613449185	1.552416864	4.114519769	78	M	WHITE	T2	N1
TCGA-MX-A5UG-01	113	1	4.392655653	4.484464997	4.625206065	78	M	ASIAN	T3	N1
TCGA-MX-A5UJ-01	600	0	4.143349107	2.286213065	3.833726098	86	F	WHITE	T3	N2
TCGA-MX-A663-01	300	1	5.060636151	2.653217472	4.842627272	66	M	WHITE	T3	N0
TCGA-R5-A7O7-01	1389	0	5.224360058	1.05719837	4.152780699	51	M	WHITE	T3	N1
TCGA-R5-A7ZE-01	554	1	3.779051297	0.561165321	5.258229564	66	F	WHITE	T3	N2
TCGA-R5-A7ZF-01	259	1	3.780747984	2.389936038	5.363085069	65	F	BLACK	T4	N1
TCGA-R5-A7ZI-01	2267	0	3.691080174	1.003574713	3.904865787	44	F	WHITE	T4	N1
TCGA-R5-A805-01	281	1	4.769500001	1.788945769	4.715200926	71	M	WHITE	T3	N2
TCGA-RD-A7BS-01	336	1	5.119702567	2.065611583	4.690631466	46	M	WHITE	T3	N1
TCGA-RD-A7BT-01	262	1	4.960715127	1.726121648	5.366335011	66	M	ISLAND ER	T3	N3

TCGA-RD-A7BW-01	156	1	3.806377518	3.574279839	4.925019227	68	F	WHITE	T2	N0
TCGA-RD-A7C1-01	507	1	3.645351764	1.693587129	5.383789928	82	M	WHITE	T2	N0
TCGA-RD-A8MV-01	3720	0	4.595533206	2.362820088	4.65939467	56	M	WHITE	T3	N2
TCGA-RD-A8MW-01	1153	1	5.987506244	1.969930947	4.379358712	72	M	WHITE	T3	N2
TCGA-RD-A8N0-01	1236	0	3.836920998	3.576454803	4.216457319	53	F	WHITE	T3	N2
TCGA-RD-A8N1-01	3519	0	5.405343443	3.25372858	4.601513959	70	M	WHITE	T3	N2
TCGA-RD-A8N2-01	3540	0	2.849990498	3.800664428	4.067357265	59	F	WHITE	T2	N0
TCGA-RD-A8N4-01	2171	0	3.44091973	3.544490345	4.269995941	58	F	WHITE	T3	N1
TCGA-RD-A8N5-01	1747	1	3.654119243	1.534152049	4.309573915	78	M	WHITE	T3	N1
TCGA-RD-A8N6-01	272	1	5.784384499	2.487566728	4.732434095	78	F	WHITE	T2	N2
TCGA-RD-A8N9-01	1083	0	4.283415456	2.578457599	4.331282933	63	F	ASIAN	T2	N1
TCGA-RD-A8NB-0	513	1	3.734014119	2.950783548	4.517437878	80	F	WHITE	T3	N1

1										
TCGA-SW-A7EA-01	579	0	5.030448361	1.157751738	5.093197676	61	F	WHITE	T2	N0
1										
TCGA-SW-A7EB-01	176	0	4.818665672	2.321407298	4.703538993	45	M	WHITE	T3	N2
1										
TCGA-VQ-A8DU-01	166	1	4.44505604	0.953980847	5.253533829	63	M	WHITE	T3	N2
1										
TCGA-VQ-A8DV-01	403	1	4.114493945	0.393517698	4.76460587	48	M	WHITE	T2	N0
1										
TCGA-VQ-A8DZ-01	396	1	4.792135686	1.380533664	4.921878573	70	M	BLACK	T4	N3
1										
TCGA-VQ-A8E0-01	562	1	5.400483607	0.97607266	5.035406528	68	M	BLACK	T3	N2
TCGA-VQ-A8E2-01	1319	0	5.816363659	2.381592175	5.26413731	57	M	ASIAN	T3	N2
TCGA-VQ-A8E3-01	661	1	4.887741365	2.344153257	4.623597582	79	M	WHITE	T3	N0
TCGA-VQ-A8E7-01	1138	0	4.951801335	0.949555245	4.49565267	59	M	WHITE	T3	N1
TCGA-VQ-A8P2-01	1160	0	4.649238747	3.351173319	4.40857418	68	M	WHITE	T4	N1
TCGA-VQ-A8P3-01	1132	0	4.139393113	1.494394588	4.501008185	72	M	WHITE	T4	N1
TCGA-VQ-A8P5-01	235	1	5.894568629	1.423836432	4.729640668	67	M	WHITE	T3	N0
TCGA-VQ-A8P8-01	942	0	3.476499544	2.853001907	4.606517007	72	F	BLACK	T4	N0
TCGA-VQ-A8PB-01	1043	1	5.065626713	2.264359599	4.021834337	65	F	WHITE	T3	N0
1										
TCGA-VQ-A8PC-01	1407	1	4.052250862	3.262354872	5.488371443	65	M	WHITE	T3	N1

1										
TCGA-VQ-A8PD-01	496	1	3.997181341	3.753474439	4.651732003	69	M	WHITE	T4	N3
1										
TCGA-VQ-A8PE-01	675	1	6.449150216	2.075776369	5.593349266	78	M	WHITE	T3	N3
1										
TCGA-VQ-A8PH-01	389	1	5.510676149	2.254706967	4.75533806	62	M	WHITE	T3	N3
1										
TCGA-VQ-A8PK-01	543	1	7.146753706	0.811834707	5.205084574	58	M	WHITE	T3	N3
1										
TCGA-VQ-A8PM-01	57	1	4.496105347	2.753835807	4.083803915	56	M	WHITE	T4	N3
1										
TCGA-VQ-A8PO-01	282	1	4.838322734	3.34786322	4.120842872	74	M	WHITE	T4	N0
1										
TCGA-VQ-A8PQ-01	476	1	4.100776701	5.220198828	4.946119146	50	F	WHITE	T4	N1
1										
TCGA-VQ-A8PU-01	832	1	6.038285992	1.211789358	4.666345585	72	F	WHITE	T4	N1
1										
TCGA-VQ-A91A-01	1200	0	4.785194777	2.125752475	4.896570571	67	M	WHITE	T3	N3
1										
TCGA-VQ-A91D-01	356	1	6.016230819	2.434999884	4.027526701	70	M	WHITE	T4	N2
1										
TCGA-VQ-A91E-01	664	0	5.145906147	2.263248797	4.129844595	67	F	WHITE	T4	N0

TCGA-VQ-A91K-01	1862	0	4.32715143	1.979372522	4.607601779	69	M	WHITE	T3	N1
TCGA-VQ-A91S-01	1000	0	5.846644091	3.806727666	4.675946255	63	M	BLACK	T4	N1
TCGA-VQ-A91U-01	52	1	6.203165838	2.684083358	4.863163933	78	M	ASIAN	T3	N1
TCGA-VQ-A91X-01	289	1	5.221948114	1.451098565	4.623686631	74	M	WHITE	T3	N2
TCGA-VQ-A91Y-01	296	1	4.769122994	3.33469025	4.885507941	67	M	WHITE	T4	N3
TCGA-VQ-A91Z-01	1690	0	6.270270661	0.887503325	4.482885534	67	F	WHITE	T3	N1
TCGA-VQ-A923-01	61	1	5.96566349	2.978966647	4.495699972	90	M	WHITE	T3	N1
TCGA-VQ-A925-01	138	1	5.650034827	1.384401777	5.044645207	66	M	WHITE	T3	N2
TCGA-VQ-A927-01	200	1	4.374627626	1.821099295	4.43361476	81	M	WHITE	T3	N3
TCGA-VQ-A928-01	174	1	5.383738102	1.725492059	4.564777435	49	M	WHITE	T3	N3
TCGA-VQ-A92D-01	2032	0	6.491225654	1.391018334	4.866419796	67	M	WHITE	T2	N0
TCGA-VQ-A94O-01	640	1	6.380374813	2.265678498	4.833763891	74	M	BLACK	T4	N3
TCGA-VQ-A94R-01	1294	1	5.458010727	2.629267621	4.053633036	63	M	WHITE	T4	N2
TCGA-VQ-A94U-01	819	0	5.167203123	2.35922798	4.224852083	70	M	WHITE	T4	N0

TCGA-VQ-AA64-01	560	1	5.624768501	1.830034342	5.714984718	68	M	WHITE	T3	N2
TCGA-VQ-AA68-01	1328	0	6.194859583	2.370143214	5.14818164	52	F	WHITE	T4	N3
TCGA-VQ-AA69-01	864	0	5.355770502	3.495625194	5.488736539	35	M	WHITE	T3	N2
TCGA-VQ-AA6A-01	1184	0	4.552639373	1.281745821	4.615350518	56	M	WHITE	T4	N3
TCGA-VQ-AA6F-01	1646	0	5.232741356	2.340446723	4.692764005	57	M	WHITE	T3	N1
TCGA-VQ-AA6G-01	792	1	6.212329318	0.736278589	5.160380746	68	M	WHITE	T3	N0
TCGA-VQ-AA6J-01	838	0	6.604678612	2.333104537	5.388446926	75	M	BLACK	T4	N2
TCGA-VQ-AA6K-01	378	1	4.756395605	1.891050054	4.983173994	59	M	WHITE	T4	N3
TCGA-ZA-A8F6-01	525	0	4.146327653	3.370547388	4.502332218	71	M	WHITE	T2	N0
TCGA-ZQ-A9CR-01	24	1	4.930574395	1.449357521	4.545435425	79	F	WHITE	T4	N3